

Surface Plasmon Enhanced Fluorescence of Dye Molecules on Metal Grating Films

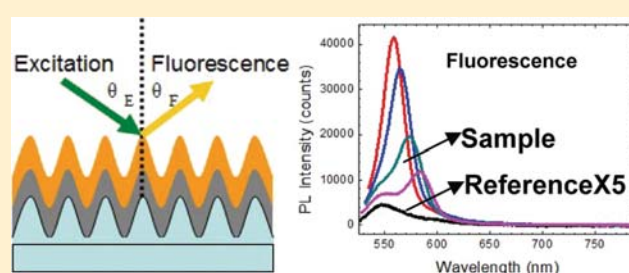
Ying Jiang,[†] Hai-Yu Wang,^{*,†} Hai Wang,^{†,‡} Bing-Rong Gao,[†] Ya-wei Hao,^{†,‡} Yu Jin,[†] Qi-Dai Chen,[†] and Hong-Bo Sun^{*,†,‡}

[†]State Key Laboratory on Integrated Optoelectronics, College of Electronic Science and Engineering, Jilin University, 2699 Qianjin Street, Changchun 130012, China

[‡]College of Physics, Jilin University, 119 Jiefang Road, Changchun 130023, China

S Supporting Information

ABSTRACT: Fluorescence enhancement of Rhodamine 6G (R 6G) molecules with a maximal enhancement factor of more than 30-fold was observed on Ag grating films. The enhancement mechanisms arise from both the surface plasmon polariton (SPP) enhanced absorption and surface plasmon coupled emission (SPCE). Time-resolved transient absorption spectroscopy was carried out to first experimentally confirm the SPP-enhanced absorption spectra of R 6G and its angle dependence on metal gratings, which cannot be directly obtained from conventional steady-state measurements. Combined with photoluminescence measurements, we observed how the contributions from two enhancement mechanisms to fluorescence emission varied with excitation incident angle and grating period. For larger grating period, the SPP-enhanced absorption becomes weaker and SPCE turns to the dominant mechanism for fluorescence enhancement. The wavelength resolution ability of SPCE makes it useful for potential applications such as wavelength-ratiometric measurements and fluorescence sensing.



INTRODUCTION

Surface plasmon polaritons (SPPs) are electromagnetic surface modes associated with collective electron oscillation propagating along the interface between a metal and a dielectric.^{1,2} In general, the excitation of SPPs is not possible on a smooth metallic surface because of the momentum mismatch between the wave vector of the SPPs and that of incident light. However, this mismatch can be overcome by an external appropriate structure on the metal surface such as gratings,¹ a prism in the Kretschmann configuration³ or an optical fiber coupled light to a plasmonic waveguide.⁴ The electromagnetic field associated with SPPs is a maximum at the interface and decays exponentially along the directions perpendicular to it. Such evanescent character of SPPs shows some unique properties, including strong electromagnetic field enhancement, extraordinary transmission, and high sensitivity to the adjacent dielectric environment, all of which make SPPs attractive for potential applications in numerous fields such as photovoltaic,^{5,6} optical/circuit elements,^{7–12} plasmon lasers,^{13–16} biosensors,¹⁷ and surface enhanced Raman Scattering as well as fluorescence emission.^{18,19}

Surface plasmon enhanced fluorescence of emitters located in the metallic vicinity has been paid special attention in recent years and mainly applied for improving the efficiency of OLED devices and increasing fluorescence detection sensitivity.^{20–28} There are two possible mechanisms for fluorescence enhancement. One is the surface plasmon induced absorption enhancement of emitters due to the enhancement of the local electric

field at the metal nanostructure interface, thus leading to fluorescence increase.² Another mechanism is surface plasmon coupled emission (SPCE),^{29–32} which is achieved by coupling the emission energies to surface plasmon modes and then reradiated to free space by scattering of the metal nanostructures. However, both enhancement mechanisms may exist in the same given system, and also because the surface enhanced absorption of molecules by SPPs cannot be directly obtained from conventional steady-state measurements, it is still necessary to experimentally confirm the contributions of absorption for fluorescence enhancement and how the two mechanisms affect the emission in the same system by tuning the SPP modes of metal nanostructures. The ultrafast laser technique is a powerful optical tool that has been widely used in laser micromanufacturing^{33,34} as well as various nonlinear optical phenomenon³⁵ and is also an ideal tool for investigating the above photophysical processes.

In this paper, we show the fluorescence enhancement of Rhodamine 6G (R 6G) molecules on Ag grating films by SPPs. The obtained maximal fluorescence enhancement factor is more than 30-fold. We find both SPP-enhanced absorption and SPCE mechanisms exist in the given system, and their contributions to fluorescence enhancement vary with incident angle and grating

Received: April 15, 2011

Revised: May 19, 2011

Published: May 24, 2011

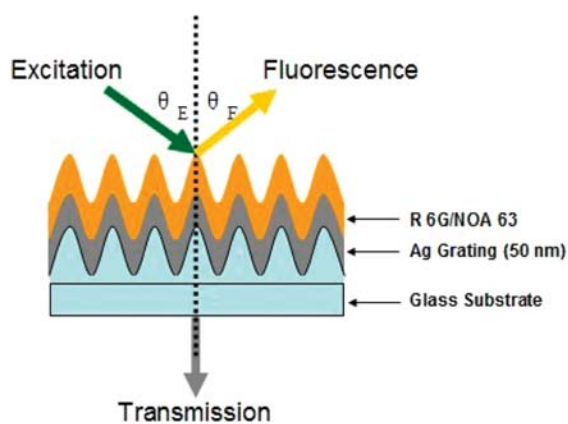


Figure 1. Sample structure of Rhodamine 6G (R 6G) coated on Ag grating films.

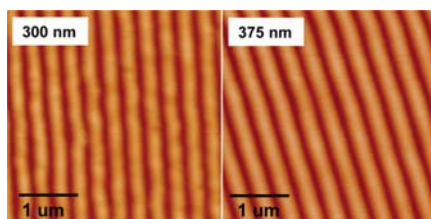


Figure 2. Atomic force microscopy (AFM) images of gratings with different periods: (a) 300 nm; (b) 375 nm.

period, respectively. Here time-resolved transient absorption spectroscopy was adopted for the first time to experimentally prove the enhanced absorption spectra of R 6G on Ag grating films by SPPs and how they along with the corresponded dynamics change with the excitation incident angle and grating period; however, all of them cannot be directly obtained from conventional steady-state measurements. Also we calculate the absorption enhancement factor from experimental data and its dependence of incident angle, which helps us to define the incident angle that produces maximal absorption to achieve the strongest fluorescence emission on a certain metal grating film. SPCE is also the main mechanism for fluorescence enhancement of R 6G on metal grating films, indicated by the angle dependence of fluorescence emission with modified radiative lifetimes as well as the larger emission enhancement of R 6G with weaker absorption enhancement on the same metal grating film. Also the wavelength resolution ability of SPCE makes it useful for many applications such as wavelength-ratiometric measurements and fluorescence sensing.

EXPERIMENT

The sample structure is shown in Figure 1. A layer of R 6G molecules doped in NOA-63 polymer resist was spin coated on top of the Ag grating film. The gratings were fabricated on NOA-63 polymer resist coated on glass substrates by the two-beam interference method. Figure 2 shows the atomic force microscopy (AFM) images of gratings with 300 and 375 nm periods. The depth of the grating was 65 nm. Before positioning the molecules, a 50 nm thick layer of silver was evaporated on top of the grating (evaporation rate 1 Å/s in a UHV chamber). Then R 6G doped polymer resist was spin coated on it (3000 rpm),

with the absorption peak at 540 nm and emission peak at 550 nm. The thickness of the dye layer is around 70 nm. The sample structure was fixed on a rotational setup for angle dependence measurements.

For the transmission measurement, a p-polarized coherent white light source as the incident light irradiated the sample with an incident angle θ . Transmission spectra were collected from the substrate side by a highly sensitive spectrometer (Avantes AvaSpec-2048 \times 14) at different incident angles θ . Similarly, the photoluminescence spectra were detected from the R 6G side by changing the collective angle θ_F with a fixed excitation incident angle θ_E . The wavelength of the p-polarized excitation source was 532 nm. Time-resolved transient absorption spectra and fluorescence dynamics were obtained by femtosecond transient absorption spectroscopy and time-correlated single photon counting (TCSPC) technology that were described in other publications.^{36,37} Briefly, femtosecond transient absorption spectroscopy was performed as follows. Twenty-five percent of the laser pulse energy, centered at 800 nm with 100 fs pulse width and a repetition rate of 250 Hz, was used to generate a white light continuum as the probe beam by focusing the beam into a 1 cm water cell. The p-polarized 530 nm excitation source generated from an optical parametric amplifier (OPA) was modulated by a synchronized optical chopper with a frequency of 125 Hz as the pump beam to excite the sample. Time-resolved transient absorption spectra were recorded with a highly sensitive spectrometer. The dynamic traces were obtained by controlling the relative delay between the pump and the probe pulses with a stepper-motor-driven optical delay line. The group velocity dispersion of the whole experimental system was compensated by a chirp program. For the TCSPC measurements, a 400 nm picosecond diode laser with a repetition rate of 20 MHz was used to excite the samples. The fluorescence was collected by a photomultiplier tube connected to a TCSPC board.

RESULTS AND DISCUSSION

Optical measurements consist of transmission, transient absorption, and photoluminescence were performed for R 6G coated on 300 and 375 nm Ag grating substrates, respectively. R 6G coated on bare grating substrates were as reference samples to eliminate the effect of grating interference.

TRANSMISSION PROPERTIES

First, we measured the transmission properties of the sample structures. Figure 3 shows the dispersion relations of transmission peaks as functions of incident angles θ for R 6G coated on 300 and 375 nm Ag grating films, respectively. The insets correspond to the transmission spectra varying with θ . As shown in Figure 3a, the peaks split into new peaks that move in opposite directions with θ increasing for the 300 nm Ag grating structure. For the 375 nm Ag grating structure, long wavelength transmission peaks red shift out of the spectrum window at relative larger angles due to the limited spectral range of white light; thus we only observe the obvious short wavelength peaks blue shift with angles. Such unique transmission properties are the result of interaction between light and SPPs. SPPs are the collective oscillation of surface charges at the metal/dielectric interface, which can be excited when their wavevector matches that of incident photon and grating as follows:

$$K_{\text{spp}} = K_0 \sin \theta \pm nK_g \quad (1)$$

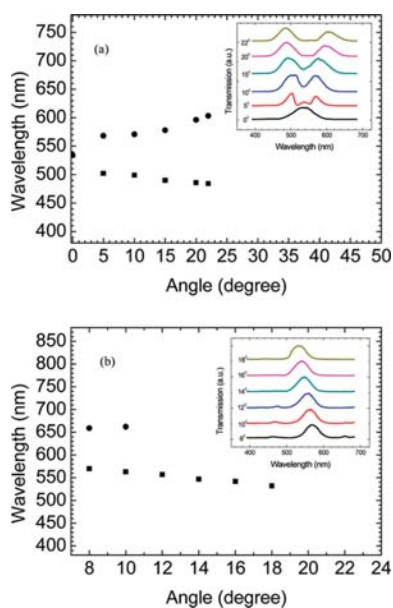


Figure 3. Dispersion relations of transmission peaks as functions of the incident angle θ for R 6G coated on Ag grating films. Grating periods: (a) 300 nm; (b) 375 nm. The insets correspond to the transmission spectra varying with θ .

where K_{spp} is the surface plasmon polaritons wavevector, $K_0 \sin \theta = (2\pi/\lambda) \sin \theta$ is the in-plane wavevector of the incident photon, $K_g = 2\pi/G$ is the grating wavevector, G is the grating period, and n is an integer that defines the order of the scattering process. Therefore when the incident angle θ is varied, the incident light can excite different SPP modes. Then we obtain the dispersion relation shown in Figure 3 by recording the peak wavelengths as a function of angle θ . In the following discussion, we will further confirm that the structure supports SPP modes and can effectively enhance the absorption and fluorescence of R 6G coated on it.

■ ABSORPTION ENHANCEMENT

It is normally accepted that there are two coupling modes between SPPs and dye molecules: weak coupling and strong coupling. The interaction between SPPs and R 6G is mainly weak coupling due to the broad absorption band of R 6G, though a strong coupling mode was reported before in certain conditions.^{38,39} The weak coupling mainly enhances the absorption and fluorescence of dyes by SPPs. Generally, it is difficult to directly observe the SPP-enhanced absorption of dyes from steady-state measurements due to the relative low concentrations of dyes and the disturbance of the SPP absorption spectrum. Thus the enhanced absorption is often reflected by the fluorescence enhancement measurements. Here for the first time we used transient absorption spectroscopy, a powerful tool to selectively excite the dye, and conveniently observed the effect of SPPs on absorption properties, which provided direct experimental evidence for SPP-enhanced absorption spectra of dye molecules on metal grating films.

Figure 4a shows the transient absorption spectra of R 6G coated on 300 nm Ag grating substrate for different excitation incident angles θ_E at 0.8 ps. The dark square line represents the transient absorption spectrum of R 6G coated on glass substrate

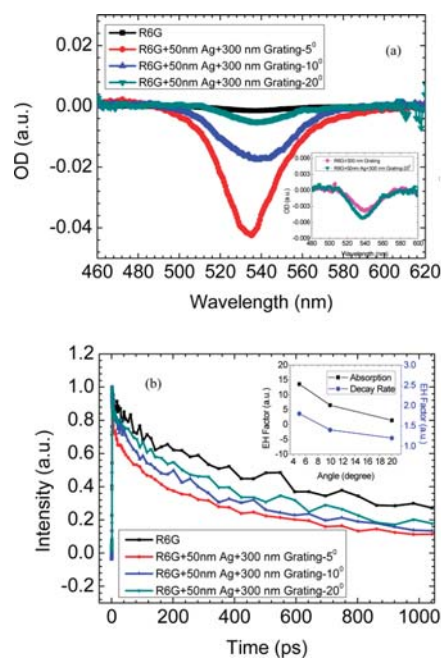


Figure 4. Transient absorption spectra (a) and the corresponding dynamics of the bleach peak at 539 nm (b) for R 6G coated on 300 nm Ag grating film at different excitation incident angles θ_E . From bottom to top, the excitation angles θ_E are 5° (red circle line), 10° (blue up triangles line), and 20° (celadon down triangle line). The excitation energy is 42 nJ pulse⁻¹. The inset in (a) shows the absorption spectrum of R 6G coated on 300 nm Ag grating film at $\theta_E = 20^\circ$ (celadon down triangle line) and that of R 6G coated on bare 300 nm grating film (pink diamond line), respectively. The inset in (b) shows the SPP-enhanced absorption (dark square line) and decay rate (blue circle line) factors as functions of excitation angles by eliminating the grating interference effect.

with bleach peak at 539 nm corresponding to its steady-state absorption peak. As shown in the figure, we observed the absorption amplitudes of R 6G coated on 300 nm Ag grating films are much larger than that of R 6G coated on glass film. The absorption peak (red circle line) achieves the maximum at $\theta_E = 5^\circ$ and then decreases gradually with the angle increased. At $\theta_E = 20^\circ$, the decreased absorption amplitude (celadon down triangle line) approaches that of R 6G coated on bare 300 nm grating film (pink diamond line), as shown in the inset of Figure 4a, but still larger than that of R 6G coated on glass substrate. Here we should note that the interference of bare grating can also increase the absorption of R 6G. Thus the absorption enhancement of R 6G coated on Ag grating substrate arises from two aspects: (1) grating interference increased absorption, while this effect is relative small; (2) SPP-enhanced absorption, which is the dominant component in the absorption enhancement and which originates from the SPP-enhanced incident field at the metal interface. And the angle dependence of absorption enhancement is due to the tunable coupling strength between the SPPs and excitation incident light in transient absorption measurements by the rotation angle. R 6G coated on bare grating film was as the reference sample to eliminate the grating interference effect on absorption enhancement. By using the integral absorption area of R 6G on the 300 nm Ag grating film divided by that of R 6G on baring 300 nm grating film, we obtained the maximal absorption enhancement factor, approaching 14-fold, and it decreased gradually

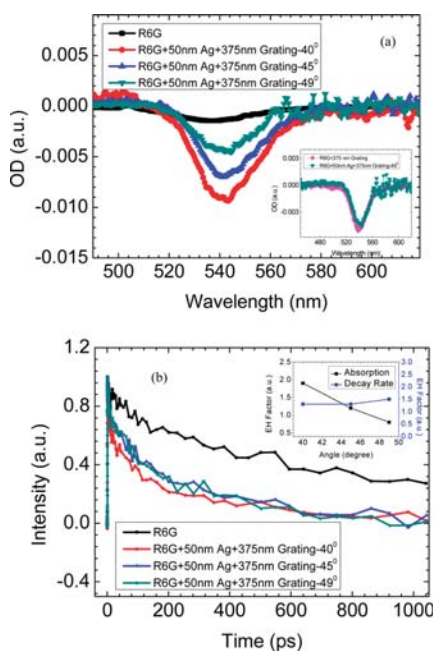


Figure 5. Transient absorption spectra (a) and the corresponding dynamics of the bleach peak at 539 nm (b) for R 6G coated on 375 nm Ag grating film at different excitation incident angles θ_E . The description is the same as that of Figure 4.

with the angle due to the smaller enhancement of the excitation incident field by SPPs with the increased angle (inset in Figure 4b, dark square line).

Figure 4b shows the absorption dynamics of the bleach peak at 539 nm with different excitation angles corresponding to Figure 4a. The dynamics shows the fastest decay rate at $\theta_E = 5^\circ$ and then slower decay with increased angle. Actually, the dynamics approaches that of R 6G coated on bare 300 nm grating film when $\theta_E = 20^\circ$ but still faster than the dynamics of R 6G coated on glass substrate (dark square line), which is consistent with the transient absorption spectra discussed above. It is due to the grating interference also increasing the excitation field, thus leading to faster dynamics even though the SPP enhancement disappeared. And it also agrees with the excitation power dependence of the absorption for R 6G, with the stronger excitation power corresponding to the larger absorption amplitude and faster decay rate, as shown in Figure 6a. However, the dynamics of R 6G coated on bare grating films shows no angle dependence within our angle range (data not shown). So the angle dependence of dynamics for R 6G coated on 300 nm Ag grating film arises from the angle dependence of the SPP-enhanced excitation field. As for smaller angles, the SPP-enhanced excitation field is stronger corresponding to the larger absorption and faster decay rate, as shown in Figure 4. Also the angle dependence of the decay rate enhancement factor is consistent with that of the absorption enhancement factor. The inset in Figure 4b shows the SPP-enhanced average decay rate with the angle (blue circle line) by taking the R 6G coated on bare 300 nm grating film as the reference sample to eliminate the interference effect, and the maximal decay rate enhancement factor is around 2-fold at 5° , corresponding to the maximal absorption enhancement factor at the same angle (~ 14 -fold at 5°).

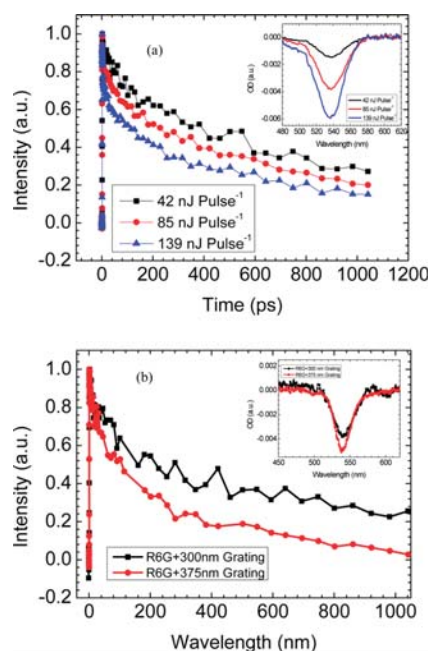


Figure 6. (a) Excitation power dependence of the dynamics at 539 nm and the transient absorption spectra (inset) for R 6G coated on bare glass substrate. From top to bottom, the excitation power energies are 42 nJ pulse^{-1} (dark square line), 85 nJ pulse^{-1} (red circle line), and $139 \text{ nJ pulse}^{-1}$ (blue up triangles line). (b) Dynamics at 539 nm and transient absorption spectra (inset) for R 6G coated on 300 nm (dark square line) and 375 nm (red circle line) bare grating films, respectively.

Similarly, the transient absorption spectra of R 6G coated on 375 nm Ag grating film has analogous absorption enhancement and excitation angle dependence (as shown in Figure 5a). However, the SPP-enhanced absorption is obviously smaller than that of R 6G coated on 300 nm Ag grating film due to the weaker coupling strength between the excitation field and the red-shifted SPP absorption spectrum of the 375 nm Ag grating. So the corresponding dynamics shows no obvious angle dependence (Figure 5b). However, the slowest dynamics of R 6G coated on the 375 nm grating film is still faster than that of R 6G coated on bare glass film (dark square line in Figure 5b), which originates from the grating interference enhanced by the excitation field as discussed above. And the interference of the 375 nm grating is stronger than that of the 300 nm grating, with a faster decay rate and larger absorption amplitude, as shown in Figure 6b. Also the fluorescence emission of R 6G coated on bare 375 nm grating is stronger than that of R 6G coated on bare 300 nm grating in our photoluminescence measurements due to the stronger interference. The SPP-enhanced absorption (dark square line) and decay rate (blue circle line) factors as functions of angles by eliminating the grating interference effect are shown in the inset of Figure 5b, respectively. The maximal SPP-enhanced absorption factor is only 2-fold, much smaller than 14-fold for R 6G coated on 300 nm Ag grating film. Thus the corresponding SPP-enhanced decay rate shows little angle dependence.

From the above results, we further confirm that our sample structure supports SPP modes, and first experimentally obtained SPP-enhanced absorption and decay rate factors as functions of excitation incident angles and their grating period dependence. Also transient absorption spectroscopy is a useful tool to define

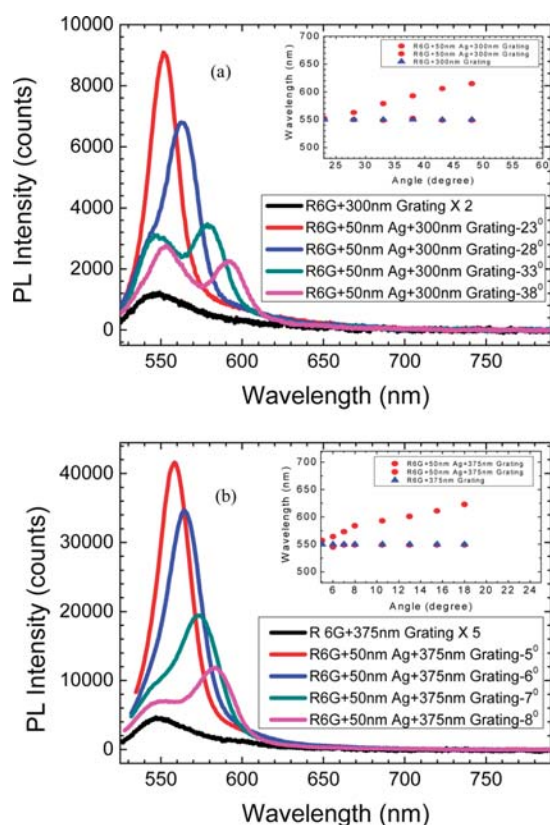


Figure 7. Fluorescence spectra of R 6G coated on Ag grating films at different detected angles θ_F with fixed excitation angles θ_E . Grating periods: (a) 300 nm; (b) 375 nm. The insets show the dispersion relations between the fluorescence peaks and detected angles.

the excitation incident angle at which maximal absorption was produced to obtain strongest fluorescence emission. In the following discussions, we will also study the SPP effect on fluorescence properties of R 6G coated on 300/375 nm Ag grating films.

■ FLUORESCENCE ENHANCEMENT

According to the above discussion, we fixed the excitation incident angle which could produce maximal absorption enhancement and then measured the fluorescence spectra of R 6G on metal grating films at different detected angles θ_F . We still took the R 6G coated on bare grating films as reference samples to eliminate the grating interference induced fluorescence enhancement. Figure 7a shows the fluorescence spectrum of R 6G coated on 300 nm Ag grating film varies with the detected angle θ_F . It has obviously larger intensity than that of R 6G coated on bare 300 nm grating film (shown as the dark square line with two times of fluorescent intensity in Figure 7a). At $\theta_F = 23^\circ$, the fluorescence enhancement is maximal and the SPP-enhanced factor is 9-fold by integral area ratio and 10-fold by intensity ratio at fluorescence peak 552 nm. As θ_F increased further, the fluorescence peak at 552 nm decreased and a new fluorescence peak appeared and red-shifted gradually with the angle. We attribute this phenomenon to the surface plasmon coupled emission (SPCE). SPCE is the fluorescence emitted by R 6G coupled to SPPs that radiates to free space by scattering (the reverse process of SPPs generation). Generally, SPP-enhanced

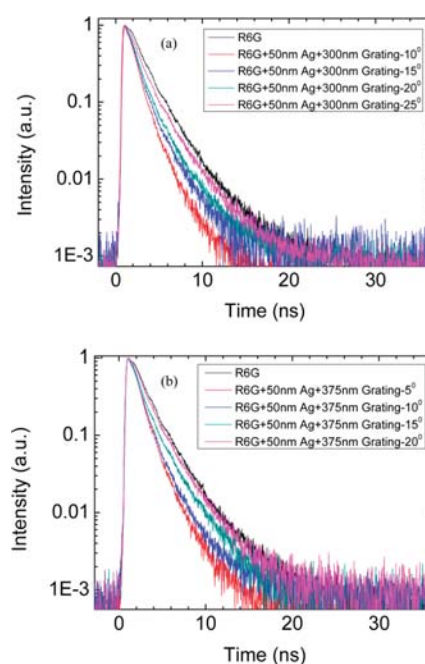


Figure 8. Detected angle dependence of the fluorescence dynamics at 550 nm by TCSPC. Grating period: (a) 300 nm; (b) 375 nm.

absorption only influences the fluorescence intensity and does not affect the spectrum shape, while SPCE not only enhances the fluorescence but also reshapes the fluorescence spectrum with a narrow band and red-shifted peak with angle, which is the result of the angle dependence of SPPs, as described in Transmission Properties. That is, different fluorescence wavelengths are amplified by SPPs at different detected angles. So we observed a new fluorescence peak that appeared and red-shifted with the increased angle. The inset in Figure 7a shows the dispersion relation between the fluorescence peak and detected angle. The dispersion curve of R 6G coated on 300 nm Ag grating film (red circles) behaves like that of SPP modes, while the fluorescence peaks are exactly the same at all detected angles for R 6G coated on bare 300 nm grating film (blue up triangles).

As for R 6G coated on 375 nm Ag grating film, it has a much more obvious fluorescence enhancement. As shown in Figure 7b, the fluorescence enhancement factor is more than 30-fold by integral area ratio and 60-fold by intensity ratio for the fluorescence peak at $\theta_F = 5^\circ$. Also the fluorescence peak red shifts more obviously. It shifts from 557 nm at 5° to 565 nm at 6° ; that is, the peak wavelength difference ($\Delta\lambda$) is 8 nm within 1° angle interval, while for R 6G coated on 300 nm Ag grating film, $\Delta\lambda$ is around 10 nm for 5° angle interval. This indicates that SPCE is more obvious for R 6G coated on 375 nm Ag grating film (also shown in the inset of Figure 7b), which mainly originates from the more spectra overlap between the fluorescence and SPPs generated by the 375 nm Ag grating. Also it is consistent with the above discussion for the weaker absorption enhancement of R 6G coated on 375 nm Ag grating film because of the weaker coupling strength between the excitation field and the red-shifted SPP modes generated by the 375 nm Ag grating. Here we should notice that the fluorescence enhancement factor by SPPs for R 6G coated on 375 nm Ag grating film though with weaker absorption enhancement is more than 3 times larger than that of R 6G coated on 300 nm Ag grating film, which indicates that

SPCE is the dominant mechanism for fluorescence enhancement of R 6G coated on 375 nm Ag grating film and it can effectively enhance the emission.

Fluorescence dynamics was also measured by TCSPC. Figure 8 shows the fluorescence dynamics of 550 nm at different detected angles. As expected, the fluorescence decay rate of R 6G coated on 300/375 nm Ag grating film is faster than that of R 6G coated on bare grating film (dark line), and it becomes slower as the angle increases. The faster decay rate is due to the stronger optical density at the metal interface induced by SPPs and also the faster rate for fluorescence coupling to SPP modes than that of fluorescence radiating to free space in the SPCE process, which was also reported in other publications.^{23–25} Note that the excitation source of TCSPC measurements is the 405 nm picosecond laser, thus the angle corresponding to the fastest decay rate is different from that with maximal fluorescence enhancement in the above photoluminescence measurements. Here we simply state that SPPs/SPCE can affect the fluorescence decay rate and anticipate that there will be a more obviously modified fluorescence lifetime with the angle under 532 nm excitation because of the much higher excitation efficiency of 532 nm than that of 405 nm for R 6G molecules.

The above results show that SPPs generated by Ag grating film can enhance the fluorescence emission of R 6G molecules close to the metal surface. The enhancement mechanisms mainly arise from two aspects: (1) SPP-enhanced absorption thus resulting in fluorescence enhancement; (2) surface plasmon coupling emission (SPCE). As discussed above, when the grating period increases from 300 to 375 nm, the absorption enhancement becomes weaker and SPCE turns to the main mechanism for fluorescence enhancement. Also the wavelength resolution ability of SPCE makes it very useful for applications such as optical switches and wavelength-ratiometric measurements. Actually, we even observed the lasing phenomenon for R 6G coated on Ag grating film that did not occur for R 6G on bare grating films and the emission bandwidth is around 5 nm (as shown in the Supporting Information), which indicates metal gratings are also helpful structures to realize plasmon lasers.

CONCLUSION

In conclusion, we show the fluorescence enhancement of R 6G molecules with modified fluorescent lifetimes on Ag gratings by SPPs. The maximal fluorescence enhancement factor is 9-fold for R 6G coated on 300 nm Ag grating film and more than 30-fold for R 6G coated on 375 nm Ag grating film. The enhancement mechanisms mainly arise from two aspects: SPP-enhanced absorption by concentrating the excitation field on the metal/R 6G interface and surface plasmon coupled emission (SPCE). Transient absorption spectroscopy provides direct experimental evidence for the absorption spectra enhancement by SPPs for R 6G coated on Ag grating films and for how the absorption enhancement factor and the decay rate vary with the incident angle as well as the grating period. The largest absorption enhancement factor with corresponding fastest decay rate is around 14-fold for R 6G coated on 300 nm Ag grating film and 2-fold for R 6G on 375 nm Ag grating film. Besides absorption enhancement by SPPs, which can lead to fluorescence enhancement, another fluorescence enhancement mechanism is SPCE, which can effectively enhance the fluorescence of dye molecules on a metal grating surface, and it is the main mechanism for the much stronger fluorescence emission of R 6G coated on 375 nm Ag

gratings even though it gives a much smaller absorption enhancement as discussed above. The wavelength resolution ability of SPCE makes it a potential application in various fields like optical switches and wavelength-ratiometric measurements. Fluorescence enhancement also has numerous applications in other fields such as increasing the efficiency of OLED devices, biological sciences, biotechnology, medical diagnostics, and sensing.

ASSOCIATED CONTENT

S Supporting Information. Lasing phenomenon for R 6G coated on Ag grating film. This material is available free of charge via the Internet at <http://pubs.acs.org>.

AUTHOR INFORMATION

Corresponding Author

*E-mail: haiyu_wang@jlu.edu.cn (H.Y.W). hbsun@jlu.edu.cn (H.B.S.).

REFERENCES

- (1) Raether, H. *Surface Plasmons on Smooth and Rough Surfaces and on Gratings*; Springer: Berlin/Heidelberg, 1988.
- (2) Stefan, A. M. *Plasmonics: Fundamentals and Applications*; Springer: Berlin/Heidelberg, 2006.
- (3) Kretschmann, E.; Raether, H. *Z. Naturforsch. A* **1986**, *23*, 2135.
- (4) Stegeman, G. I.; Wallis, R. F.; Maradudin, A. A. *Opt. Lett.* **1983**, *8*, 386.
- (5) Atwater, H. A.; Polman, A. *Nat. Mater.* **2010**, *9*, 205.
- (6) Nishijima, Y.; Ueno, K.; Yokota, Y.; Murakoshi, K.; Misawa, H. *J. Phys. Chem. Lett.* **2010**, *1*, 2031.
- (7) Ditlbacher, H.; Hohenau, A.; Wagner, D.; Kreibitz, U.; Rogers, M.; Hofer, F.; Aussenegg, F. R.; Krenn, J. R. *Phys. Rev. Lett.* **2005**, *95*, 257403.
- (8) Bozhevolnyi, S. I.; Volkov, V. S.; Devaux, E.; Laluet, J. Y.; Ebbesen, T. W. *Nature* **2006**, *440*, 508.
- (9) Pacifici, D.; Lezec, H. J.; Atwater, H. A. *Nat. Photonics* **2007**, *1* (7), 402.
- (10) De Vlaminck, I.; Van Dorpe, P.; Lagae, L.; Borghs, G. *Nano Lett.* **2007**, *7*, 703.
- (11) Guo, X.; Qiu, M.; Bao, J.; Wiley, B. J.; Yang, Q.; Zhang, X.; Ma, Y.; Yu, H.; Tong, L. *Nano Lett.* **2009**, *9*, 4515.
- (12) Tian, J.; Ma, Z.; Li, Q.; Song, Y.; Liu, Z.; Yang, Q.; Zha, C.; Åkerman, J.; Tong, L.; Qiu, M. *Appl. Phys. Lett.* **2010**, *97*, 231121.
- (13) Noginov, M. A.; Zhu, G.; Belgrave, A. M.; Bakker, R.; Shalaev, V. M.; Narimanov, E. E.; Stout, S.; Herz, E.; Suteewong, T.; Wiesner, U. *Nature* **2009**, *460*, 1110.
- (14) Noginov, M. A.; Zhu, G.; Mayy, M.; Ritzo, B. A.; Noginova, N.; Podolskiy, V. A. *Phys. Rev. Lett.* **2008**, *101*, 226806.
- (15) Ma, R. M.; Oulton, R. F.; Sorger, V. J.; Bartal, G.; Zhang, X. *Nat. Mater.* **2011**, *10*, 110.
- (16) Oulton, R. F.; Sorger, V. J.; Zentgraf, T.; Ma, R. M.; Gladden, C.; Dai, L.; Bartal, G.; Zhang, X. *Nature* **2009**, *461*, 629.
- (17) Anker, J. N.; Hall, W. P.; Lyandres, O.; Shah, N. C.; Zhao, J.; Van Duynne, R. P. *Nat. Mater.* **2008**, *6*, 442.
- (18) Yokota, Y.; Ueno, K.; Misawa, H. *Small* **2011**, *7*, 252.
- (19) Barnes, W. L. *J. Mod. Opt.* **1998**, *45*, 661.
- (20) Neumann, T.; Johansson, M. L.; Kambhampati, D.; Knoll, W. *Adv. Funct. Mater.* **2002**, *12*, 575.
- (21) Ray, K.; Badugu, R.; Lakowicz, J. R. *J. Am. Chem. Soc.* **2006**, *128*, 8998.
- (22) Zhang, X.; Wang, P.; Zhang, X.; Xu, J.; Zhu, Y.; Yu, D. *Nano Res.* **2009**, *2*, 47.
- (23) Song, J. H.; Atay, T.; Shi, S.; Urabe, H.; Nurmikko, A. V. *Nano Lett.* **2005**, *5*, 1557.

- (24) Wang, Y.; Yang, T.; Pourmand, M.; Miller, J. J.; Tuominen, M. T.; Achermann, M. *Opt. Exp.* **2010**, *18*, 15560.
- (25) Kwon, M. K.; Kim, J. Y.; Kim, B. H.; Park, I. K.; Cho, C. Y.; Byeon, C. C.; Park, S. J. *Adv. Mater.* **2008**, *20*, 1253.
- (26) Tanaka, K.; Plum, E.; Ou, J. Y.; Uchino, T.; Zheludev, N. I. *Phys. Rev. Lett.* **2010**, *105*, 227403.
- (27) Zeng, Q.; Zhang, Y.; Liu, X.; Tu, L.; Wang, Y.; Kong, X.; Zhang, H. *Chem. Commun.* **2010**, *46*, 6479.
- (28) Ito, F.; Ohta, R.; Yokota, Y.; Ueno, K.; Misawa, H.; Nagamura, T. *Chem. Lett.* **2010**, *39*, 1218.
- (29) Lakowicz, J. R. *Anal. Biochem.* **2004**, *324*, 153.
- (30) Gryczynski, I.; Malicka, J.; Gryczynski, Z.; Lakowicz, J. R. *Anal. Biochem.* **2004**, *324*, 170.
- (31) Lakowicz, J. R. *Anal. Biochem.* **2005**, *337*, 171.
- (32) Lakowicz, J. R.; Ray, K.; Chowdhury, M.; Szmajcinski, H.; Fu, Y.; Zhang, J.; Nowaczyk, K. *Analyst* **2008**, *133*, 1308.
- (33) Wu, D.; Chen, Q. D.; Niu, L. G.; Wang, J. N.; Wang, J.; Wang, R.; Xia, H.; Sun, H. B. *Lab Chip* **2009**, *9*, 2391.
- (34) Xu, B. B.; Xia, H.; Niu, L. G.; Zhang, Y. L.; Sun, K.; Chen, Q. D.; Xu, Y.; Lv, Z. Q.; Li, Z. H.; Misawa, H.; Sun, H. B. *Small* **2010**, *6*, 1762.
- (35) Zhao, J. H.; Cheng, B. W.; Chen, Q. D.; Su, W.; Jiang, Y.; Chen, Z. G.; Jia, G.; Sun, H. B. *IEEE Photon J.* **2010**, *2*, 974.
- (36) Jiang, Y.; Wang, H. Y.; Xie, L. P.; Gao, B. R.; Wang, L.; Zhang, X. L.; Chen, Q. D.; Yang, H.; Song, H. W.; Sun, H. B. *J. Phys. Chem. C* **2010**, *114*, 2913.
- (37) Gao, B. R.; Wang, H. Y.; Hao, Y. W.; Fu, L. M.; Fang, H. H.; Jiang, Y.; Wang, L.; Chen, Q. D.; Xia, H.; Pan, L. Y.; Ma, Y. G.; Sun, H. B. *J. Phys. Chem. B* **2010**, *114*, 128.
- (38) Cade, N. I.; Ritman-Meer, T.; Richards, D. *Phys. Rev. B* **2009**, *79*, 241404.
- (39) Hakala, T. K.; Toppari, J. J.; Kuzyk, A.; Pettersson, M.; Tikkanen, H.; Kunttu, H.; Törmä, P. *Phys. Rev. Lett.* **2009**, *103*, 053602.